Transformation of Atomically Dispersed Platinum in SAPO-37 into Platinum Clusters: Catalyst for Ethylene Hydrogenation

SCHOLARONE™
Manuscripts

Transformation of Atomically Dispersed Platinum in SAPO-37 into Platinum Clusters: Catalyst for Ethylene Hydrogenation

Jorge E. Perez-Aguilar,[a] James T. Hughes,[b]* Cong-Yan Chen,[a,c] and Bruce C. Gates[a]*

[a]Department of Chemical Engineering, University of California, Davis, CA 95616, United States
[b]Zeolyst International, Conshohocken, PA 19428, United States
[c]Chevron Technical Center, Richmond, CA 94802, United States

Abstract

Atomically dispersed supported platinum catalysts were synthesized by the reaction of $Pt(acac)_2$ (acac = acetylacetonato) with the silicoaluminophosphate molecular sieve SAPO-37, with infrared spectra showing that the reaction involved SAPO OH groups. Extended X-ray absorption fine structure (EXAFS) spectra show that, after heating in air to 623 K, each platinum atom on average was bonded to approximately two oxygen atoms of the SAPO support, with no evidence of platinum clusters. X-ray absorption near edge spectra (XANES) indicate a platinum formal oxidation state of approximately +2. These supported mononuclear species lacked catalytic activity for ethylene hydrogenation at 1 bar and room temperature, but activity arose during catalysis in a once-through flow reactor/X-ray absorption spectroscopy cell, as the XANES white line intensity decreased, indicating reduction of the platinum, and the EXAFS-determined Pt−Pt coordination number (CN) increased from essentially zero to 2.7 ± 0.5 after 2 h, indicating the formation of platinum clusters of only a few atoms each. The data indicate the almost instantaneous formation of the clusters and identify them as the catalytically active species. Subsequent exposure of the catalyst to ethylene as *in-situ* EXAFS and XANES data were recorded led to a decrease in the Pt−Pt coordination number to 1.6 ± 0.3 and an increase in the white line intensity, indicating partial oxidative fragmentation of the clusters by ethylene. Platinum clusters in SAPO-37 formed in separate experiments by exposure to H_2 prior to catalysis were also catalytically active for ethylene hydrogenation. The data thus show how to dial in the catalytic activity by forming platinum clusters by exposure of mononuclear

platinum to H_2 and how to dial back the activity by oxidative fragmentation of the clusters by reaction with ethylene, all under mild conditions; the ethylene:H_2 ratio of the reactant gas determines the average platinum nuclearity and thus the catalytic activity.

1. Introduction

Zeotype materials are widely used as acid-base catalysts for the production of fuels, petrochemicals, and fine chemicals,[1–3] and they find wide applications as supports for catalytic metals, with applications including hydrocracking,[4] hydroisomerization,[5,6] reforming (aromatization),[7,8] and vehicle exhaust abatement.[9,10] Both support chemical properties such as acidity and physical properties such as aperture and cage dimensions affect the catalyst performance, as illustrated by data characterizing alkane hydroisomerization and reforming (e.g., in the Chevron Aromax™ process) catalyzed by platinum in zeolites.[11,12] The physical properties of the crystalline zeotype supports offer numerous advantages, including high surface areas for high metal dispersions, structures that stabilize metals including iridium[13] and platinum[14] in highly dispersed states by encapsulation,[15]–in pores that facilitate shape-selective catalysis[16] and limit metal sintering at high temperatures.[17] The crystalline nature of these supports also offers the prospective advantages of structural uniformity of the supported species to facilitate fundamental understanding of the structure and function of the catalytic species.[18] Zeolite-supported platinum catalysts are used on a large scale in some of the aforementioned applications.[19] Practical advantages include high hydrogenation selectivities observed for platinum nanoparticles encapsulated in MFI zeolites[20] and high selectivity for isomerization of alkanes (*n*-pentane and *n*-hexane) observed for platinum clusters supported on micro/mesoporous ZSM-5.[21] Recent work has been focused on highly dispersed (even atomically dispersed) platinum in zeolites,[22,23] with part of the motivation being the advantages of high metal utilization efficiency, maximized influence of the support, and new properties of noble metals in the most highly dispersed state, when they are positively charged.[24] Yet there are hardly any data allowing comparisons of zeolites with other zeotype materials as supports, and there is a lack of elucidation of the chemistry of metal cluster formation and its reverse in atmospheres other than H_2 and O_2, respectively.

Our goal was fundamental understanding of the role of a non-zeolite support for an atomically dispersed noble metal catalyst. We chose platinum supported on the silicoaluminophosphate molecular sieve SAPO-37,[25,26] because platinum is of wide importance in catalysis and because SAPO-37 has the same framework structure as zeolite Y and thus provides the opportunity for comparisons with that zeolite to help elucidate the role of the support composition on catalyst performance. Because SAPOs incorporate framework phosphorus atoms, they behave differently from their zeolite counterparts as supports, as illustrated for atomically dispersed rhodium catalyzing the conversion of ethylene in the presence of H_2.[27]

Our specific goals were to investigate highly dispersed platinum supported on SAPO-37 as a catalyst for the reaction of ethylene with H_2; a working hypothesis was that the catalyst structures would be simple and uniform enough to yield to insights into the structure of the catalytic species and how to control them.

The precursor used for catalyst synthesis was bis(acetylacetonato)platinum(II), $Pt(acac)_2$, chosen because it offers the prospect of making atomically dispersed platinum by reaction with support OH groups. Ethylene hydrogenation was chosen as the catalytic test reaction to take advantage of the smallness of the reactant molecules to allow access to catalytic sites within pores and of the identifiable spectroscopic signatures of the reactants and the adsorbed species derived from them.

2.   Materials and Methods

2.1 Preparation of Catalysts by Reaction of Pt(acac)₂ with SAPO-37

Platinum complexes were anchored to SAPO-37 that was synthesized by a reported method,[27] with the precursor $Pt(acac)_2$ reacting with SAPO-37 powder that had been calcined at 873 K for 6 h in flowing air (Praxair, 99.5% purity) followed by 6 h under dynamic vacuum in a once-through plug-flow reactor. Sample handling and treatments were carried out with standard air-exclusion techniques. Under an argon atmosphere, the precursor $Pt(acac)_2$ (6.0 mg, 98 wt%, Strem) was mixed thoroughly with 300.0 mg of the calcined SAPO-37 powder and placed in the flow reactor. The reactor tube was evacuated and then sealed under vacuum. The temperature was ramped up to 333 K at 1 K min^{-1} and held for 1 h, then ramped further to 353 K and held for 1 h, under vacuum (there was no flow through the reactor during this procedure).

After further ramping to 373 K, the catalyst was held at this temperature for 1 h as the $Pt(acac)_2$ powder in the mixture with the SAPO-37 particles sublimed and was deposited onto the SAPO-37.[28] If all the platinum in the precursor $Pt(acac)_2$ were deposited in the SAPO-37, the platinum loading would have been 1.1 wt%. The resultant catalyst was then exposed to air flowing at 45 mL(NTP) min^{-1}, and the temperature was ramped to 403 K at a rate of 1 K min^{-1} and held for 15 min, followed by a further temperature ramp (1 K min^{-1}) to 623 K and a 2-h soak.[29] The resulting sample was recovered and stored in an argon-filled glovebox.

2.2. Elemental Analysis of Supported Platinum Catalyst

The platinum content of the SAPO-37-supported platinum sample was determined at the University of California Davis Interdisciplinary Center for Plasma Mass Spectrometry with an Agilent Model 7500a, quadrupole-type, inductively coupled plasma mass spectrometer (ICP-MS) (Agilent Technologies, Santa Clara, CA).

2.3. Infrared (IR) Spectroscopy

A Bruker IFS 66v spectrometer with a room-temperature DTGS detector and a spectral resolution of 2 cm^{-1} was used to collect transmission IR spectra of the catalyst samples. Approximately 10 mg of powder was pressed between two KBr windows for optical optimization that allowed detection of minor peaks. IR spectra were recorded with samples at room temperature under vacuum, with each spectrum being an average of 128 scans. In some experiments, the sample was placed in a diffuse reflectance (DRIFTS) reaction chamber (Harrick Scientific) equipped with KBr windows, mounted in a Praying Mantis diffuse reflectance adapter (Harrick Scientific). The cell in the argon-filled glovebox was loaded with approximately 50 mg of dry KBr powder (Crystal Labs, 7758-02-3), along with 15 mg of catalyst sample on top of the KBr powder. This cell was connected into a flow system without exposure of the sample to air, and it allowed recording of spectra as reactant gases (CO, ^{13}CO, O_2, D_2, H_2, and/or ethylene) flowed through the cell at the desired temperature.

2.4. X-Ray Absorption Spectroscopy (XAS)

X-ray absorption spectroscopy (XAS) experiments characterizing the platinum-containing samples were carried out at beam lines 4-1 and 9-3 of the Stanford Synchrotron Radiation Lightsource (SSRL). In an argon-filled glovebox at SSRL, powder samples were loaded into a transmission fluorescence X-ray absorption spectroscopy cell/flow reactor[30] or a Kapton capillary (1.0 mm OD) cell and held in place with quartz wool.[31] The storage ring energies and currents were 3 GeV and 500 mA, respectively. X-ray energy scans from −250 to 1000 eV relative to the Pt L_{III} edge (11564 eV) were obtained by using a double-crystal Si(220) monochromator at each beamline. For calibration purposes, measurement of the absorption of a platinum foil mounted downbeam of the sample was carried out simultaneously. Transient fluorescence X-ray absorption near edge spectra (XANES) and extended X-ray absorption fine structure (EXAFS) spectra were collected for samples in flowing reactive gases in a once-through flow system, with the effluent gases characterized with an online mass spectrometer (Hiden Analytical QGA) downstream of the cell. The following m/z values were used to identify the products: m/z = 28 for ethylene; 30 for ethane; and 41 for butenes.

Analysis of the EXAFS data was carried out with the Athena software of the Demeter package and with the software XDAP.[32] Athena was used for edge calibration and deglitching and XDAP for background removal, normalization, and conversion of the data into an EXAFS function file. Reference files used in the fitting, with backscattering amplitudes and phase shifts for Pt–Pt, Pt–O, Pt–C, and Pt–Al contributions, were calculated with the software FEFF7.0 from crystallographic coordinates of the unit cells of the reference compounds platinum metal, PtO_2, $Pt(acac)_2$, and Pt-Al alloy.[33,34] Each analyzed spectrum was the average of four spectra. Details of the data processing and analysis methodology are reported elsewhere.[27] The quality of each fit was evaluated by the goodness of fit, defined as follows:

$$Goodness\ of\ fit = \frac{\nu}{NPTS(\nu - N_{free})}\sum_{i=1}^{NPTS}\left(\frac{\chi_{exp,i} - \chi_{model,i}}{\sigma_{exp,i}}\right)^2$$

where χ_{exp} and χ_{model} are the experimental and calculated EXAFS functions, respectively; σ_{exp} the error in the experimental results; ν the number of independent data points in the fit range; N_{free} the number of free parameters; and NPTS the number of data points in the fit range. The estimates of the (approximate) error

bounds are based on the reported results and statistical analyses. Best-fit models of each of EXAFS data set were fitted initially with various combinations of plausible absorber–scatterer contributions, which led to a list of candidate models. Then, a "difference-file" technique was applied to assess the candidate models, whereby the calculated EXAFS contribution from each individual Pt–scatterer contribution was compared with the data in R (distance) space. This iterative fitting was continued in R space for both overall and individual contributions with the Fourier-transformed EXAFS data (χ data) until the best-fit model was obtained, which is the one providing optimum agreement between the calculated k_0-, k^1-, k^2-, and k^3-weighted EXAFS data and the model.

2.5. Catalytic Activity Measurements

Catalyst performance was tested with samples in a once-through temperature-controlled plug-flow reactor. The equipment and procedures have been described in detail.[27] The feed gases helium, H_2, and ethylene with the following partial pressures (in mbar) were as follows: 50 for ethylene; 50 for H_2; 900 for helium or, alternatively, 10 for ethylene; 100 for H_2; 890 for helium. The gas stream flowed through a bed of catalyst particles of mass typically 1.0–2.0 mg mixed with 0.5 g of particles of inert, nonporous α-Al_2O_3 (Sigma Aldrich, 100–200 mesh) at atmospheric pressure, a temperature of 303 K, and a total feed flow rate of 100 mL(NTP) min^{-1}. The effluent stream was analyzed periodically with an online gas chromatograph (Hewlett−Packard 6890N) equipped with a capillary column (PLOT Alumina "M," 50 m × 0.53 mm) and a flame ionization detector. All the reported catalytic reaction rates were determined from differential conversions and expressed per platinum atom (turnover frequencies, TOF) recorded at various times on stream. The maximum activity, following an induction period of typically 2.5 h, was observed before the onset of substantial catalyst deactivation. The conversions were <10% and shown to be differential on the basis of the essentially linear dependences of conversion on inverse space velocity (e.g., Fig. S1 in the Supplementary Material, SM).

2.6 Summary of Characterization Experiments

Scheme 1 in the SM is a summary of the characterization techniques that were used to investigate the samples, including experiments done after treatments of the SAPO-37-supported platinum in various gas atmospheres.

3. RESULTS

3.1. Synthesis of SAPO-37-Supported Platinum

During the first step of the catalyst synthesis, as $Pt(acac)_2$ (which is yellow) was thoroughly mixed with the SAPO-37 and vaporized, there was no observable color change in the SAPO-37. The subsequent oxidation treatment during the synthesis led to a change in color of the material from white to green. These observations are consistent with the incorporation of platinum in the SAPO-37. The elemental analysis data show that the SAPO-37 contained 1.1 ± 0.1 wt% platinum, consistent with the masses of $Pt(acac)_2$ and SAPO-37 used in the synthesis and the inference that all of the precursor $Pt(acac)_2$ reacted with the SAPO-37 support. The lack of observation of any deposits formed from the precursor during the synthesis and the color change of the SAPO-37 bolster this conclusion. This platinum loading corresponds to approximately 1 platinum atom per 25 supercages.

Changes in the IR spectra of the samples indicate that SAPO Si–OH–Al sites (Brønsted acid sites) were converted by reaction with the platinum precursor. Spectrum A of Fig. 1 represents bare SAPO-37 calcined at 873 K in air followed by evacuation; spectrum B represents the sample after the synthesis that involved chemisorption of $Pt(acac)_2$ and subsequent oxidation. The intensities of the bands at 3640 and 3578 cm^{-1} corresponding to the SAPO Si–OH–Al sites (in supercages and sodalite cages, respectively)[35,36] decreased as the platinum species evidently became bonded at these sites. IR spectra of the sample (Fig. S2 in SM) indicate that after the oxidation synthesis (details in Section 2.1), the acac ligands had been removed, presumably in the synthesis, as shown by the lack of ν_{COring}, $\nu_{C–C–Cs}$, and δ_{CH} vibrations expected if Hacac had remained on the support as a product of the chemisorption.[27] Further, the data provide no evidence of acac ligands remaining on the platinum after this treatment. The bands corresponding to the SAPO Si–OH (3745 cm^{-1}) and P–OH (3675 cm^{-1}) sites and the hydroxyls in the minor extra-framework (3718 cm^{-1})

7

components of the support were too low in intensity to justify any conclusions about whether the precursor reacted with them.[37–40]

3.2. EXAFS Spectra of Isolated Platinum Complexes and Clusters Formed from them on SAPO-37

EXAFS data recorded near the Pt L_{III} edge provide structural information about the platinum-containing SAPO-37 sample. A substantial Pt L_{III} absorption edge intensity confirmed the presence of platinum in the sample. Fitting of the data (Table 1, Fig. 2a) demonstrated a lack of measurable Pt–Pt scattering (consistent with atomic dispersion of the platinum bonded to SAPO-37) and a Pt–light scatterer contribution, with a coordination number of nearly 4 at an average distance of 2.02 Å (a bonding distance, such as a Pt–O bonding distance). The IR data show that support OH groups were converted in the synthesis when the Pt(acac)$_2$ was chemisorbed and the sample was subsequently oxidized; the data imply that the platinum was bonded through Pt–O$_{support}$ bonds. The EXAFS data also give evidence of another Pt–light-scatterer contribution, with a coordination number of nearly 2 at a distance of 2.29 Å (longer than a typical Pt–O bonding distance) (Table 1). We suggest that the support provided two oxygen ligands for each platinum atom, comparable to HY zeolite as a support for atomically dispersed cationic rhodium and iridium, and that the other scatterers represent ligands formed in the oxidation step of the synthesis that is expected to have removed the acac.[27,41] To check whether some platinum clusters might have formed in the synthesis, we investigated a candidate structural model in the EXAFS data fitting that included a Pt–Pt contribution. However, no satisfactory fit could be obtained with such a model.

But fitting of the EXAFS data recorded after the sample (150 mg) had been exposed to flowing H$_2$ (50 mL(NTP) min^{-1}) for 1 h demonstrates the formation of Pt–Pt bonds, implying the breaking of Pt–O bonds and unlinking of platinum from the support—that is, reduction, migration, and aggregation of platinum and the formation of platinum clusters. The EXAFS data characterizing the H$_2$-reduced sample (Table 1) demonstrate that the Pt–Pt coordination number increased from a value indistinguishable from zero to about 4, accompanied by a decrease in the Pt–light scatterer coordination number from about 4 to about 1 as more

platinum atoms were unlinked from the support. These clusters, on average, are several-atom clusters (Table 1).

Others have made similar observations of platinum clusters in zeotype materials; for example, Torigoe *et al.*[42] and Moliner *et al.*[43] found CNs similar to ours after exposure of chabazite-supported atomically dispersed platinum to H_2 at 773 K and suggested cluster diameters in the range of 1.0–1.3 nm.[43] We hypothesize that hydride ligands formed on platinum as clusters formed, but any gas-phase products formed in the reduction were evolved in concentrations too low to observe with the online mass spectrometer.

Species comparable to the atomically dispersed platinum species present initially on the SAPO-37 support have been reported to exist in zeolites KLTL, NaY, and NaX, with these supports typically acting as bidentate ligands that provide two oxygen atoms to anchor each platinum atom.[22,44,45] A summary of the EXAFS data characterizing this family of samples is given in Table 1.

Table 1. Structural Models Based on EXAFS Spectra Characterizing Initial Platinum Complexes Supported on SAPO-37 and on Various Zeolites.[a]

Form of catalyst	Shell[b]	N	R (Å)	$10^3 \times \sigma^2$	ΔE_0 (eV)	Ref.
Pt/SAPO-37, 1.1 ± 0.1 wt% platinum	Pt−O$_s$	4.0	2.02	5.9	-8.0	this work
	Pt−O$_l$	2.0	2.29	2.4	-1.0	
	Pt−Al	1.0	2.70	1.8	-8.0	
	Pt−O$_l$	2.5	2.99	5.0	2.8	
Pt/SAPO-37, 1.1 ± 0.1 wt% platinum, after exposure to H_2 for 30 min	Pt−O$_s$	1.0	2.03	11.8	-8.0	
	Pt−Pt	4.0	2.71	3.8	-8.0	
	Pt−O$_L$	1.0	3.43	6.8	-1.7	
	Pt−Al	1.1	3.97	4.8	-4.0	
PtO$_x$/KLTL zeolite (oxidized), 1.0 wt% platinum	Pt−N	0.6	2.00	1.2	-1.8	[22]
	Pt−O$_s$	2.8	2.01	8.9	-3.8	
	Pt−O$_l$	5.9	2.64	10.5	8.0	
	Pt−Al	1.1	3.19	2.6	11.3	
0.2 wt% Pt/NaY zeolite	Pt−O$_s$	2.3	2.01	8.67	4.1	[44]
6 wt% Pt/NaY zeolite	Pt−O$_s$	3.9	2.03	7.4		[45]
	Pt−O$_l$	0.9	3.03	3.9	-3.93	
	Pt−Al/Si	0.6	3.52	5.9		
6 wt% Pt/NaX zeolite	Pt−O$_s$	3.8	2.04	7.4		[45]
	Pt−O$_l$	2.1	3.07	3.2	-3.30	
	Pt−Al/Si	0.7	3.20	4.5		
0.33 wt% Pt/CHA zeolite	Pt−O$_s$	3.22	2.01	1.6	12.4	[43]

[a]Notation: *N*, coordination number; *R*, distance between absorber and scatterer atoms; σ^2, disorder term; ΔE_0, inner potential correction. Error bounds (accuracies) characterizing the structural parameters determined by fitting the EXAFS spectra are estimated to be as follows: *N*, ±20%; *R*, ±0.02 Å; σ^2, ±20%; ΔE_0, ±20 %. Details of the EXAFS fitting are provided in the SM. [b]The subscripts s and l refer to short and long, respectively.

3.3. XANES of Platinum Complexes on SAPO-37 and Clusters formed by their Reduction in H_2

XANES data recorded with the EXAFS data are compared with those of reference compounds: platinum metal foil (characterizing Pt^0); solid $Pt(acac)_2$ (characterizing Pt^{2+}); and solid PtO_2 (characterizing Pt^{4+}) (Fig. 2b). The white-line intensity increased in the order Pt foil < SAPO-37-supported platinum clusters < $Pt(acac)_2$ < SAPO-37-supported isolated platinum complexes < PtO_2, consistent with the trends in the platinum formal oxidation states (but we refrain from assigning values of formal oxidation states of platinum in the supported samples on the basis of XANES data alone, as these data also depend on the platinum coordination). The data (Fig. 2) also indicate that the white line intensity characterizing each of the supported platinum complexes was slightly greater, and shifted to higher energy (eV), relative to that of the precursor $Pt(acac)_2$, demonstrating that the platinum in the initial SAPO-37-supported species was cationic. A comparison of the magnitude of the Fourier transform of the initial SAPO-37-supported platinum complexes with that of platinum foil (Fig. 2b) shows a single major contribution at 2.0 Å and no evidence of Pt–Pt bonding, which would have been indicated by a contribution at 2.7 Å matching that in the spectrum of platinum foil. However, when the supported sample was exposed to H_2, the magnitude of the Fourier transform characterizing the EXAFS spectra at 2.7 Å (indicating a Pt–Pt contribution) increased (Fig. 2b, Table 1). Thus, the initial platinum species on SAPO-37 were isolated cationic species that were reduced in H_2 and converted to platinum clusters.

3.4. Reactivity of Atomically Dispersed Supported Platinum Species Characterized by IR Spectroscopy

To further investigate the reactivity of the platinum species on SAPO-37, samples (20 mg) in the DRIFTS cell were brought in contact first with N_2 flowing at a rate of 50 mL(NTP) min^{-1} at atmospheric pressure and 298 K and then with a 12-min pulse of CO flowing at a rate of 50 mL(NTP) min^{-1} at atmospheric pressure and 298 K (2390 CO molecules per platinum atom). The sample in a flowing stream

of 10% O_2 in helium (50 mL(NTP) min^{-1}) was then heated at a rate of 5 K min^{-1} to 473 K as spectra were

recorded. Spectrum A in Fig. 3, characterizing the sample in flowing N_2 prior to exposure to CO, includes

two sets of ν_{CO} bands (at 2123 and 2090 cm^{-1}) characterizing the initially prepared sample (after the

oxidation step). We infer that the CO present initially (Fig. S3 in the SM) had formed from the acac ligands

in the Pt(acac)$_2$ precursor that reacted to form CO on the platinum species. But such species were minor

components, as confirmed by the EXAFS data (Table 1) demonstrating that, on average, platinum was

bonded predominantly to ligands that we suggest incorporated light scatterers, including two oxygen atoms

of the support characterized by the shorter Pt–O distance.[46–48] Spectrum B (Fig. 3) shows that the same

sample in N_2 after exposure to a 15-min CO pulse included several new bands in the region of 2220–2090

cm^{-1}. These ν_{CO} bands characterizing the sample after reaction with CO indicate isolated platinum species

characterized by various CO coordinations and/or platinum in various formal oxidation states, as indicated

by results reported for platinum carbonyls on zeolites.[45,49,50]

   As the temperature subsequently increased with the sample in flowing O_2 at atmospheric pressure

(Spectrum C), the intensities of the bands initially evident in the 2220–2090 cm^{-1} region decreased. This

result is consistent with the expectation that the CO ligands were removed by oxidation, but the mass

spectrometer used to analyze the effluent stream was not sensitive enough to detect any evolved CO_2.

Spectrum D, recorded after oxidation at 473 K with the sample in flowing N_2 at room temperature, includes

a remaining single ν_{CO} peak, at 2134 cm^{-1}, indicating differing reactivities of the CO ligands. For

comparison, Table S2 in the SM is a summary of data characterizing carbonyls of platinum in various

formal oxidation states (0 to +3) and with various coordination numbers (1 to 3) on various zeolites. These

data show that both the local coordination and formal platinum oxidation state influence the ν_{CO} values.

The IR data are not sufficient by themselves to identify the platinum species,[51] but the XANES spectra

exclude the possibility that the initial supported species (after the oxidation step in the synthesis)

incorporated zero-valent platinum (details in SM) and include the possibility of platinum bonded to 1 or

more CO ligands.

To further investigate the reactivity of the supported platinum and its local environment on SAPO-37, samples (20 mg) in the DRIFTS cell were brought in contact with helium flowing at 50 mL(NTP) min^{-1} at atmospheric pressure and 298 K. The sample was then exposed to H_2 flowing at 50 mL(NTP) min^{-1} at atmospheric pressure and 298 K for 30 min, and then the H_2 was purged out of the cell with helium, and the sample was exposed to a 12-min CO pulse (2392 CO molecules per platinum atom). The ν_{CO} region of the spectrum (Fig. S4 in SM) includes a single band at 2092 cm^{-1} in the range expected for CO on platinum clusters.[49] The results thus verify the EXAFS data characterizing the sample after the H_2 exposure, which show that platinum clusters had formed (Table 1, Table S3 in SM). Correspondingly, they verify the XANES data demonstrating reduction of the platinum as clusters formed (Fig. 2b).

The reduction was carried out separately with D_2 instead of H_2: the initially prepared platinum-containing sample was exposed to helium flowing at 50 mL(NTP) min^{-1} at atmospheric pressure and 298 K and then exposed to D_2 flowing at 10 mL(NTP) min^{-1} at atmospheric pressure and 298 K (Fig. S5 in the SM). The SAPO-37 OH group bands shifted from 3718, 3640, and 3578 cm^{-1} to 2766, 2686, and 2642 cm^{-1}, and, consistent with the harmonic oscillator approximation, the new bands are assigned to surface OD groups.[52] Thus, spillover occurred, with D_2 evidently activated on the platinum clusters and D migrating and undergoing exchange with support OH groups.[53,54]

When the Pt-containing sample containing OD groups was exposed to ethylene flowing at 10 mL(NTP) min^{-1} (Fig. S5 in the SM), ethylene adsorbed on the OD and OH groups; when the reactor was purged with helium, the ethylene desorbed, as shown by the full recovery of the OH and OD band intensities (Fig. S5 in the SM). These results indicate adsorption of ethylene on the OH or OD groups, consistent with reported results.[55]

3.5. Catalytic Performance of Supported Platinum: Evidence of Formation of Platinum Clusters as Catalytically Active Species

In experiments with a wide range of ethylene conversions in the presence of H_2, ethane was the only observed product. There was no detectable conversion when the SAPO-37 sample was present without platinum: the platinum was responsible for the catalysis.

The conversion initially increased with time on stream in the flow reactor, Fig. 4 (the catalyst mass was 1.0 mg, the feed flow rate 100 mL(NTP) min^{-1}, and the C_2H_4 and H_2 partial pressures 10 and 100 mbar, respectively). Catalyst break-in such as this is commonly associated with changes in the metal–ligand environment resulting from reaction with the reactants, as illustrated by data of Martinez-Macias et al.,[56] who characterized changes in zeolite-supported iridium complexes during the break-in period. These authors did not determine how the ligands changed during this period, but they systematically varied the ligands present before catalysis (Ir(CO)(C$_2$H$_4$) and Ir(C$_2$H$_4$)$_2$ in HY zeolite) and demonstrated that the activity depended strongly on them, with the initial activities being in the order Ir(CO)$_2$ << Ir(CO)(C$_2$H$_4$) < Ir(C$_2$H$_4$)$_2$ and the induction periods decreasing in the order (Ir(CO)$_2$ > Ir(CO)(C$_2$H$_4$) > Ir(C$_2$H$_4$)$_2$).[56]

Our results show that after an induction period of increasing activity (2.5 h), catalyst deactivation ensued, and, after about 172 h, the catalyst had lost essentially all of its activity (Fig. 4). The number of turnovers during this period was approximately 913,000.

To test the hypothesis that the changes in the catalyst were associated with changes in the reactant-derived ligands—that would be expected to proceed faster at higher reactant partial pressures—we did an experiment with the same catalyst mass and feed flow rate but feed partial pressures of C_2H_4 and H_2 of 40 and 400 mbar (instead of 10 and 100 mbar), respectively. Correspondingly, the induction time was markedly reduced (Fig. S6 in the SM), and the catalyst deactivated more rapidly (in about 144 h), consistent with the expectation. The results show that reactant-derived species caused the deactivation.

A summary comparison of the activities of these and related catalysts investigated under similar conditions is shown in Table 2.

Realizing that atomically dispersed platinum on numerous supports is easily reduced and aggregated and that platinum clusters and nanoparticles are active for our reaction,[43,57,58] we did complementary experiments with a catalyst incorporating preformed platinum clusters, made by pretreating the as-prepared

sample in H_2 flowing at 50 mL(NTP) min^{-1} at room temperature for 1 h prior to the start of flow of ethylene + H_2 (Section 2.1). Thus, after a helium purge to remove H_2, the catalyst was tested under conditions matching those stated above (1.0 mg catalyst; feed flow rate 100 mL(NTP) min^{-1} ; and C_2H_4 and H_2 partial pressures of 40 and 400 mbar, respectively). The deactivation profile was similar to that observed with the catalyst that had not been pre-reduced, with the activities estimated by extrapolation to zero time on stream (ignoring the induction period) being approximately the same and indistinguishable from each other within the estimated error (Table 2, Fig. S6 in the SM). Comparable activity data for platinum nanoparticles supported on SBA-15 silica, SiO_2, and Al_2O_3 are listed in Table 2. For comparison, data characterizing atomically dispersed rhodium and atomically dispersed iridium supported on DAY zeolite are shown with data characterizing SAPO-37 in Table 2.

Table 2. Comparison of Activities of Catalysts Incorporating Metal Complexes Supported on SAPO-37, Alumina, DAY Zeolite, and Silica for Hydrogenation of Ethylene.

Metal in catalyst	Support	Metal loading, wt%	initial form of catalyst	TOF (s^{-1})	ref.
Platinum	SAPO-37	1.1 ± 0.1 wt%	Atomically dispersed platinum species	0.12[a,b]	this work
				3.0[a,c]	
				4.5 ± 0.5[d]	
			Platinum clusters	6.6 ± 2.0[d]	
	SBA-15 silica	1.0	Platinum nanoparticles	0.64[e]	57
	SiO$_2$	0.05		1.3[f]	57
		0.5		17.5[f]	57
	Al$_2$O$_3$	9.2		53.4[f]	57
Iridium	DAY zeolite	1.0	Ir(C$_2$H$_4$)$_2$	0.71[g]	56
Rhodium			Rh(C$_2$H$_4$)$_2$	0.10[h]	27
	SAPO-37		Rh(C$_2$H$_4$)$_2$	0.13[h]	

[a]TOFs determined at maximum activity reached after induction period and before catalyst deactivation at respective conditions (Fig. 4). The errors in the TOF values are estimated to be ± 10%, determined primarily by the error in the platinum content of the catalyst.
[b]TOFs determined at maximum activity at 303 K and 1.0 bar; feed partial pressures (mbar): C_2H_4, 50; H_2, 50; helium, 900; total flow rate 100 mL(NTP)/min; catalyst mass, 11.0 mg.
[c]TOFs determined at maximum activity at 303 K and 1.0 bar; feed partial pressures (mbar): C_2H_4, 10; H_2, 100; helium, 890; total flow rate 100 mL(NTP)/min; catalyst mass, 0.5–1.5 mg.

[d]Initial TOFs determined from C_2H_4 conversions <5%; catalyst mass, 1 mg; feed partial pressures (mbar): C_2H_4, 40; H_2, 400; helium, 560; total flow rate, 100 mL(NTP)/min.
[e]Steady-state TOF determined at 298 K; feed partial pressures (mbar): C_2H_4, 10; H_2, 100; inert, 890; catalyst mass, 1.1 mg.
[f]Rates reported as calculated from reported data,[57] which are corrected to 10 mbar C_2H_4, 100 mbar H_2, and 298 K; see reference for details.
[g]Steady-state TOF determined at 303 K; feed partial pressures (mbar): C_2H_4, 100; H_2, 200; helium, 700.
[h]Initial TOFs determined from C_2H_4 conversions <5%; catalyst mass, 10−30 mg; feed partial pressures (mbar): C_2H_4, 50; H_2, 50; helium, 900; total flow rate, 100 mL(NTP)/min.

3.6. XAS of Isolated Platinum Complexes and Platinum Clusters in Reactive Atmospheres

XAS experiments were done to characterize the SAPO-37-supported platinum in various atmospheres at various temperatures and during catalysis. XANES and k^3-weighted Fourier-transformed EXAFS data are shown in Figs. 5a and b, respectively, recorded as the catalyst underwent changes in structure influenced by changes in the flowing gas atmosphere, with the products measured by on-line mass spectrometry: spectrum A represents the initial atomically dispersed platinum in flowing helium and spectrum B the sample after subsequent exposure to flowing ethylene—which evidently caused the white line to decrease in intensity and shift to a higher energy, accompanied by a decrease in magnitude of the Fourier transform at approximately 2.0 Å. Spectrum C represents the sample after the feed stream had subsequently been switched to a mixture of ethylene + H_2 (C_2H_4:H_2 ratio = 1:10, molar), with catalysis occurring, and the data show a further decrease in the white line intensity and a slight shift of the white line to higher energy as well as a substantial increase in the magnitude of the Fourier transform at approximately 2.7 Å. Spectrum D was recorded after 2 h of exposure to catalytic reaction conditions followed by a switch of the feed again to ethylene, whereupon the white line increased in intensity and shifted to a lower energy; the Fourier-transformed data show maxima at approximately 2.1 and 2.6 Å.

In a continuation of the experimental sequence, transient data characterizing the transformation of the initial isolated platinum complexes into platinum clusters—and subsequent cluster breakup—were obtained with the catalyst in the XAS cell working as a flow reactor. Fig. 6a shows the ethane signal from the online mass spectrometer downstream of the reactor along with XAS data recorded as a function of time on stream. Fig. 6b shows transient white line and temperature data recorded during the experiments. Fig. 6c shows the

Pt−Pt distance and coordination number as a function of time onstream. When the sample was initially present in flowing helium, the magnitude of the Pt−light-scatterer contribution and the white line intensity were maximized, and no Pt−Pt contribution was observed. These data match the EXAFS data reported in Table 1. When the sample was later exposed to flowing ethylene at atmospheric pressure and room temperature (298 K), the magnitude of the Pt−light-scatterer contribution and the white line intensity decreased, and no Pt−Pt contribution was observed. We therefore conclude that the ligand sphere of the platinum had changed, consistent with the statements above and consistent with the adsorption of ethylene on the platinum. When the feed was then changed again to a reactive mixture of ethylene + H_2 (C_2H_4:H_2 ratio = 1:10, molar), the magnitude of the Pt−light-scatterer contribution decreased; the white line intensity decreased slightly; and a Pt−Pt contribution became evident and grew in intensity. The Pt−Pt coordination number jumped from 0 to 1.8, and the ethane signal in the mass spectrum increased, all within the period of the first scan (which required 5 min). These results show that platinum clusters formed in the reactive atmosphere that included H_2. As time progressed, the ethane signal in the mass spectrum increased and remained almost unchanged as the magnitude of the Pt−light-scatterer contribution decreased and the magnitude of the Pt−Pt contribution increased. We conclude from the increase in the Pt−Pt coordination number (from 1.8 to 2.7) that—as the catalytic reaction occurred—the average size and/or number of platinum clusters increased (Fig. 6c).

In a further continuation of the series of experiments with the same sample in the XAS cell, after 2 h of exposure to catalytic reaction conditions, the feed was switched back to ethylene. The data show that the magnitude of the Pt−light-scatterer contribution and the white line intensity both increased (the latter only slightly), but the values did not revert to the initial values—those observed before exposure of the catalyst to reaction conditions with ethylene + H_2 flowing. Concomitantly, the magnitude of the Pt−Pt contribution decreased, and the average Pt−Pt coordination number and distance also decreased, and—with H_2 being absent—the ethane signal decreased to noise level in the mass spectrum of the effluent.

This latter result indicates oxidative fragmentation of the platinum clusters by ethylene, which acts as an oxidizing agent[59] (ethylene has been shown to oxidatively fragment zeolite-supported clusters of iridium

and of rhodium[60]). The inference is consistent with the slight increase in white line intensity (Fig. 6c) and the decrease in Pt−Pt coordination number (2.7 to 1.6). These values indicate that, under our conditions, ethylene caused platinum cluster fragmentation but did not fragment the clusters entirely—that is, it did not cause the white line intensity to return to its initial value observed before catalytic reaction started. Further, the contraction of the average Pt−Pt bond distance from 2.74 to 2.64 Å, as H_2 was purged from the reactor and ethylene was present, matches results reported by Bus *et al.*[61] showing that platinum clusters losing hydrogen by desorption are characterized by decreasing Pt–Pt bond distances.

In the above-mentioned work,[59] it was shown that ethylene completely fragmented supported iridium clusters (consisting of approximately 4 atoms each) on a zeolite support when the sample was heated to 353 K. To check whether ethylene could similarly completely fragment the platinum clusters,[62] the same platinum-containing sample mentioned above was heated to 353 K in flowing ethylene; then it was cooled to room temperature in a period of 20 min, and the ethylene stream was replaced with helium. The white line intensity did not change during the temperature increase. Nor did purging of ethylene from the cell with helium lead to a change in the white line intensity. Consistent with these results, the average Pt−Pt coordination number was within error the same as that observed prior to the exposure of the sample to flowing ethylene as the temperature was increased and as the ethylene was later purged (Fig. 6c). We thus conclude the platinum clusters remained stable as the temperature increased 353 K with the sample in ethylene and did not undergo complete fragmentation comparable to that observed for the zeolite-supported iridium clusters.[62]

We emphasize that the platinum clusters that formed in the partial fragmentation in ethylene were smaller than the ones formed by reduction of the initially formed catalyst in flowing H_2 (Table 1), with average cluster diameters that we infer on the basis of earlier estimates[43] to be in the range of 0.4–0.8 nm—characterizing extremely small clusters, with Pt−Pt coordination numbers ranging from about 1 to 4.

In summary, the EXAFS data (Table 1 and Table S2 in SM) show that the platinum complexes present initially in the catalyst were converted into clusters within the period of the first scan under catalytic reaction conditions with H_2. As catalytic hydrogenation continued in the flow reactor, the average cluster size and/or

number of clusters increased. When these clusters were later exposed to ethylene in the absence of H_2, they fragmented, and the products included smaller clusters (Fig. 6c). During subsequent heating in the presence of flowing ethylene, the clusters were stable and not fragmented further.

Thus, all the data are consistent with the hypothesis that the observed catalytic activity is associated with the platinum clusters.

3.7. Characterization of Deactivated Catalyst

To gain insight into the catalyst activity loss, 20 mg of the catalyst following operation at room temperature, during which deactivation was essentially complete, were packed into the DRIFTS cell and exposed at 303 K and 1 bar to flowing $C_2H_4 + H_2$ at a molar ratio of 1:10. IR spectra recorded in separate experiments as the catalytic reaction proceeded (Fig. S7 in SM) show increasing intensities of peaks assigned to C−H vibrations (2970−2860 cm^{-1}), indicating carbonaceous deposits in the SAPO-37; similar results were observed for rhodium in zeolite catalysts.[27] We infer from the similar spectra that essentially the same carbonaceous deposits formed and interacted with the platinum centers, causing catalyst deactivation. Under these conditions, the initial CO peak observed at 2123 cm^{-1} declined in intensity during operation at a C_2H_4:H_2 molar ratio of 1:10, and the catalyst color changed from green to beige. After 24 h onstream, the reactants were purged from the cell with helium, and a CO pulse (50 mL(NTP)/min, 2390 CO molecules per platinum atom) was injected to provide IR evidence of whether the platinum nuclearity had changed. Fig. S8 in the SM includes the ν_{CO} region of the spectrum, showing that the initial platinum species characterized by bands at 2123 and 2090 cm^{-1} (assigned to isolated platinum complexes and clusters, respectively) reappeared in greater intensity after the CO pulse. The results imply that the catalyst had begun to undergo aggregation under the catalytic reaction conditions (C_2H_4:H_2 molar ratio of 1:10), caused by the reduction by H_2.

The experiment was essentially repeated with the catalyst in the DRIFTS cell, but with D_2 instead of H_2, with a C_2H_4:D_2 ratio of 1:10 (Fig. S9). Again, during catalytic reaction, the Si−OH−Al groups of the SAPO-37 were replaced with Si−OD−Al groups. The rate of formation of Si−OD−Al groups under catalytic

reaction conditions (C_2H_4:D_2 ratio of 1:10) was lower than that observed when pure D_2 flowed through the cell, corresponding to the lower D_2 partial pressure (165 vs. 35 min, when the Si−OD−Al absorbance stopped changing).

4. Discussion

4.1 Reaction of Pt(acac)₂ with SAPO-37 Hydroxyl Groups to form Atomically Dispersed Platinum

The characterization data all support the conclusion that Pt(acac)$_2$ reacted with Si−OH−Al Brønsted acid sites of SAPO-37, with the platinum becoming bonded through Pt–O bonds in structures comparable to those of numerous zeolite- and metal oxide-supported atomically dispersed platinum with a formal oxidation state near +2.

A remaining question is what ligands were bonded to the platinum in addition to the support. We postulate that the unidentified light scatterers could have been oxygen, with the results being similar to those reported for similarly treated atomically dispersed platinum on zeolites NaY,[44,45] NaX,[45] and chabazite,[43] but the data are not sufficient to identify them. Candidates (Scheme 1 in the SM) could be peroxo, OH, acac, and CO, but the IR spectra rule out acac and CO; a discussion of these possibilities is presented in the SM.

The IR spectra (Fig. 3) give evidence of a mixture of platinum-containing species formed when CO reacts with the initial atomically dispersed supported platinum (after the oxidation step in the synthesis), but, because CO can be a reducing agent and might have reduced platinum from its initial cationic state at room temperature, the data are not sufficient to assign CO peaks as various platinum oxidation states or CO coordinations based on reported work. Further interpretation of the CO region along with a comparison of the XANES spectra would benefit from simulations, which are beyond the scope of this work.

4.2 Formation of Platinum Clusters in SAPO-37

The XANES and EXAFS data (Fig. 2, Table 1) showing that H_2 reacted with the SAPO-37-supported platinum species at room temperature to reduce the platinum and form clusters are broadly consistent with extensive literature demonstrating such behavior of platinum on numerous zeolite[43,63] and metal oxide

supports.[64] IR spectra in the ν_{CO} region characterizing these clusters after exposure to CO (Fig. S4 in SM), consistent with the XANES and EXAFS data shown in Fig. 2 and Table S3 in the SM, agree well with data characterizing platinum clusters on zeolite H-MOR and on Al_2O_3, with a single ν_{CO} band near 2095 cm^{-1} assigned to CO ligands on platinum clusters.[65,66] Thus, we assign the 2090 cm^{-1} band (Fig. S4 in SM) to CO on these clusters.

The XANES data representing the SAPO-37-supported platinum clusters are characterized by significantly higher white line intensities than bulk platinum metal (Figs. 2b and 5a), indicating that the supported platinum species are small enough to have electronic properties significantly different from those of bulk platinum. This statement is consistent with the smallness of the clusters demonstrated by the EXAFS data.

The observation of facile platinum cluster formation implies that platinum species were mobile and that Pt–O bonds were broken to form the mobile species; the data are not sufficient to identify them, but we consider it likely that they were platinum hydrides. Results characterizing other atomically dispersed metals, exemplified by iridium on HY zeolite,[62] have led to a similar conclusion.

4.3 Reactivity of Platinum Complexes under Conditions of Ethylene Hydrogenation Catalysis

Under catalytic reaction conditions (with the sample in the presence of ethylene + H_2 or ethylene + D_2), the ligands on the platinum changed, consistent with the change in ethylene conversion and incorporation of hydrogen and ethylene ligands on the platinum. The platinum cluster formation during catalysis evidently started immediately upon exposure of the sample to H_2.[61,67] The data are consistent with results of Bus *et al.*,[61] who reported that platinum clusters on Al_2O_3 were characterized by an increase in the Pt–Pt coordination number and a changed Pt–Pt bond distance attributed to (co)adsorbed hydrogen resulting from exposure to ethylene + H_2. A key result is that the clusters are catalytically active for ethylene hydrogenation, and there is no evidence that the atomically dispersed platinum is active.

The only catalytic reaction product was ethane, so that there is no selectivity information for contrasting the isolated platinum sites and the platinum clusters—in contrast to what has been observed for supported rhodium[68] and iridium[69] catalysts.

Both atomically dispersed rhodium and rhodium clusters on HY zeolite catalyze ethylene hydrogenation,[41,68] and an equivalent statement pertains to iridium.[70] However, gold is different; MgO-supported mononuclear gold was found to be active for ethylene hydrogenation, and gold clusters that formed under catalytic reaction conditions were inactive.[71] Similar results were observed for hydrogenation of 1,3-butdiene on gold supported on ZrO_2.[72]

4.4 Platinum Cluster Formation and Redispersion and Stabilization of Clusters in SAPO-37 Pores

Recent reports of platinum at low loadings (0.1 wt%) in various zeolites[14,43] demonstrate the reduction of atomically dispersed platinum in H_2 to form clusters and the redispersion by exposure to O_2 at high temperatures.[73] The samples are robust, but the platinum species are nonuniform, with images, EXAFS, and XANES data giving evidence of structures ranging from atomically dispersed platinum to clusters in the pores to nanoparticles outside the pores. The work reported here, in contrast, involves a SAPO-37-supported catalyst with an order of magnitude higher platinum loading and transformations under much milder conditions, and during catalysis—with evidence (Fig. 6) of how to tune the relative amounts of the catalytically active and catalytically inactive species by dialing in the composition of the reactive gas environment. The chemistry reported here takes place without the involvement of metal carbonyls as intermediates, in contrast to numerous reports characterizing the formation and fragmentation of rhodium and iridium clusters in zeolite Y.[41,68,69]

5. Conclusions

IR and EXAFS spectra characterizing samples formed by the reaction of $Pt(acac)_2$ with SAPO-37 (after oxidation synthesis) show that the supported platinum was atomically dispersed, with each platinum atom initially bonded on average to two support oxygen atoms and other unidentified ligands. The atomically dispersed platinum rapidly transformed into clusters of only a few atoms each (with average diameters in the range of about 0.4–0.8 nm) upon exposure to H_2. These platinum clusters catalyzed ethylene hydrogenation with 100% selectivity at 303 K. Subsequent exposure of the clusters to ethylene led to their partial oxidative fragmentation, and these were stable at elevated temperatures. The data support the

conclusion that the clusters are the catalytically active species, with no evidence of catalytic activity by the atomically dispersed platinum. The results are the first to provide a detailed picture of the structures SAPO-37-supported metal complexes and clusters and show that the SAPO-37 has properties markedly different from those of the isostructural HY zeolite.

Appendix A. Supplementary Material

Supplementary data associated with this article can be found in the online version, at DOI#....

Notes

The authors declare no competing financial interest.

6. References and Notes

1   J.E. Naber, K.P. de Jong, W.H.J. Stork, H.P.C.E. Kuipers, M.F.M. Post, Industrial applications of zeolite catalysis, *Stud. Surf. Sci. Catal.*, 1994, **84**, 2197–2219.

2   W. Vermeiren, J.P. Gilson, Impact of zeolites on the petroleum and petrochemical industry, *Top. Catal.*, 2009, **52**, 1131–1161.

3   P.R. Robinson, C.S. Hsu, Practical Advances in Petroleum Processing, Springer: New York, 2006.

4   F. Alvarez, F.R. Ribeiro, G. Perot, C. Thomazeau, M. Guisnet, Hydroisomerization and

     hydrocracking of alkanes. 7. Influence of the balance between acid and hydrogenating functions

     on the transformation of n-decane on PtHY catalysts, *J. Catal.*, 1996, **162**, 179–189.

5   Z. Vajglová, N. Kumar, M. Peurla, L. Hupa, K. Semikin, D.A. Sladkovskiy, D.Y. Murzin, Effect

     of the Preparation of Pt-Modified Zeolite Beta-Bentonite Extrudates on Their Catalytic Behavior

     in n-Hexane Hydroisomerization, *Ind. Eng. Chem. Res.*, 2019, **58**, 10875–10885.

6   D.N. Gerasimov, V. V. Fadeev, A.N. Loginova, S. V. Lysenko, Hydroisomerization of long-chain

     paraffins: Mechanism and catalysts. Part I, *Catal. Ind.*, 2015, **7**, 128–154.

7   K.H. Steinberg, U. Mroczek, F. Roessner, Aromatization of ethane on platinum containing ZSM-5

     zeolites, *Appl. Catal.*, 1990, **66**, 37–44.

8   C. Perego, A. Carati, Zeolites: From Model Materials to Industrial Catalysts, Transworld Research

     Network: Kerala, India, 2008.

9   H.-X. Li, W.E. Cormier, B. Moden, US Patent 20190054420 A1 2019.

10   A. Wang, Y. Wang, E.D. Walter, R.K. Kukkadapu, Y. Guo, G. Lu, R.S. Weber, Y. Wang, C.H.F.

     Peden, F. Gao, Catalytic N_2O decomposition and reduction by NH_3 over Fe/Beta and Fe/SSZ-13

     catalysts, *J. Catal.*, 2018, **358**, 199–210.

11   C.M. M'Kombe, M.E. Dry, C.T. O'Connor, Influence of preparation variables on the dispersion of

     platinum on zeolite KL, *Zeolites*., 1997, **19**, 175–179.

12   J.A. Martens, D. Verboekend, K. Thomas, G. Vanbutsele, J. Pérez-Ramírez, J.P. Gilson,

     Hydroisomerization and hydrocracking of linear and multibranched long model alkanes on

     hierarchical Pt/ZSM-22 zeolite, *Catal. Today*, 2013, **218**–**219**, 135–142.

13   L. Liu, M. Lopez-Haro, D.M. Meira, P. Concepcion, J.J. Calvino, A. Corma, Regioselective

     Generation of Single-Site Iridium Atoms and Their Evolution into Stabilized Subnanometric

     Iridium Clusters in MWW Zeolite, *Angew. Chem. Int. Ed.*, 2020, **59**, 15695–15702.

14   L. Liu, D.N. Zakharov, R. Arenal, P. Concepcion, E.A. Stach, A. Corma, Evolution and

stabilization of subnanometric metal species in confined space by in situ TEM, *Nat. Commun.*, 2018, **9**, 574.

15   Y. Chen, S. Ji, C. Chen, Q. Peng, D. Wang, Y. Li, Single-Atom Catalysts: Synthetic Strategies and Electrochemical Applications, *Joule*, 2018, **2**, 1242–1264.

16   L. Liu, A. Corma, Confining isolated atoms and clusters in crystalline porous materials for catalysis, *Nat. Rev. Mater.*, 2020.

17   A.W. Petrov, D. Ferri, F. Krumeich, M. Nachtegaal, J.A. Van Bokhoven, O. Kröcher, Stable complete methane oxidation over palladium based zeolite catalysts, *Nat. Commun.*, 2018, **9**,1-8.

18   L. DeRita, J. Resasco, S. Dai, A. Boubnov, H.V. Thang, A.S. Hoffman, I. Ro, G.W. Graham, S.R. Bare, G. Pacchioni, X. Pan, P. Christopher, Structural evolution of atomically dispersed Pt catalysts dictates reactivity, *Nat. Mater.*, 2019, **18**, 746–751.

19   J. Weitkamp, L. Puppe, Catalysis and Zeolites - Fundamentals and Applications, Springer Berlin Heidelberg, 1999.

20   J. Gu, Z. Zhang, P. Hu, L. Ding, N. Xue, L. Peng, X. Guo, M. Lin, W. Ding, Platinum Nanoparticles Encapsulated in MFI Zeolite Crystals by a Two-Step Dry Gel Conversion Method as a Highly Selective Hydrogenation Catalyst, *ACS Catal.*, 2015, **5**, 6893–6901.

21   P. Tamizhdurai, P.S. Krishnan, A. Ramesh, K. Shanthi, Isomerization of hydrocarbons over Pt supported on micro-mesoporous ZSM-5, *Polyhedron*, 2018, **154**, 314–324.

22   J.D. Kistler, N. Chotigkrai, P. Xu, B. Enderle, P. Praserthdam, C.Y. Chen, N.D. Browning, B.C. Gates, A single-site platinum CO oxidation catalyst in zeolite KLTL: Microscopic and spectroscopic determination of the locations of the platinum atoms, *Angew. Chem. Int. Ed.*, 2014, **53**, 8904–8907.

23   J. Guo, C. Ding, Z. Ma, L. Ma, J. Wang, J. Shangguan, Q. Yuan, M. Zhao, Y. Li, M. Wang, K. Zhang, Highly dispersed and stable Pt clusters encapsulated within ZSM-5 with aid of sodium ion for partial oxidation of methane, *Fuel*, 2021, **289**, 119839.

24   L. Liu, D.M. Meira, R. Arenal, P. Concepcion, A. V. Puga, A. Corma, Determination of the

Evolution of Heterogeneous Single Metal Atoms and Nanoclusters under Reaction Conditions: Which Are the Working Catalytic Sites?, *ACS Catal.*, 2019, **9**, 10626–10639.

25   B.M. Lok, C.A. Messina, R.L. Patton, R.T. Gajek, T.R. Cannan, E.M. Flanigen, Silicoaluminophosphate Molecular Sieves: Another New Class of Microporous Crystalline Inorganic Solids, *J. Am. Chem. Soc.*, 1984, **106**, 6092–6093.

26   L.S. Sierra de Saldarriaga, C. Saldarriaga, M.E. Davis, Investigations into the Nature of a Silicoaluminophosphate with the Faujasite Structure, *J. Am. Chem. Soc.*, 1987, **109**, 2686–2691.

27   J.E. Perez-Aguilar, C.Y. Chen, J.T. Hughes, C.Y. Fang, B.C. Gates, Isostructural Atomically Dispersed Rhodium Catalysts Supported on SAPO-37 and on HY Zeolite, *J. Am. Chem. Soc.*, 2020, **142**, 11474–11485.

28   S.B. Hong, E. Mielczarski, M.E. Davis, Aromatization of *n*-hexane by platinum-containing molecular sieves I. Catalyst preparation by the vapor phase impregnation method, *J. Catal.*, 1992, **134**, 349–358.

29   G. Jacobs, F. Ghadiali, A. Pisanu, A. Borgna, W.E. Alvarez, D.E. Resasco, Characterization of the morphology of Pt clusters incorporated in a KL zeolite by vapor phase and incipient wetness impregnation. Influence of Pt particle morphology on aromatization activity and deactivation, *Appl. Catal. A Gen.*, 1999, **188**, 79–98.

30   A.S. Hoffman, L.M. Debefve, A. Bendjeriou-Sedjerari, S. Ouldchikh, S.R. Bare, J.M. Basset, B.C. Gates, Transmission and fluorescence X-ray absorption spectroscopy cell/flow reactor for powder samples under vacuum or in reactive atmospheres, *Rev. Sci. Instrum.*, 2016, **87**, 073108.

31   A.S. Hoffman, J.A. Singh, S.F. Bent, S.R. Bare, In situ observation of phase changes of a silica-supported cobalt catalyst for the Fischer–Tropsch process by the development of a synchrotron-compatible in situ/operando powder X-ray diffraction cell, *J. Synchrotron Radiat.*, 2018, **25**, 1673–1682.

32   M. Vaarkamp, J.C. Linders, D.C. Koningsberger, A new method for parameterization of phase shift and backscattering amplitude, *Phys. B Phys. Condens. Matter*, 1995, **208**–**209**, 159–160.

33   P. Villars, L.D. Calvert, Pearson's handbook of crystallographic data for intermetallic phases, Wiley, Metals Park, 1987.

34   K. Ha, Crystal structure of bis(pentane-2,4-dionato-κ^2O,O′) platinum(II), Pt(C$_5$H$_7$O$_2$)$_2$, *Z. Krist. New Cryst. Struct.*, 2011, **226**, 329–330.

35   A. Corma, V. Fornés, M.J. Franco, F.A. Mocholí, J. Pérez-Pariente, Hydrothermal Stability and Cracking Behavior of Silicoaluminophosphate Molecular Sieve-37 with Different Silicon Contents, *ACS Symp. Ser.*, 1991, **452**, 79–95.

36   S. Dzwigaj, M. Briend, A. Shikholeslami, M.J. Peltre, D. Barthomeuf, The acidic properties of SAPO-37 compared to faujasites and SAPO-5, *Zeolites*, 1990, **10**, 157–162.

37   M.A. Makarova, A.F. Ojo, K. Karim, M. Hunger, J. Dwyer, FTIR study of weak hydrogen bonding of brönsted hydroxyls in zeolites and aluminophosphates, *J. Phys. Chem.*, 1994, **98**, 3619–3623.

38   A. Corma, V. Fornes, J. Pérez-Pariente, SAPO-37: The implications of structure flexibility on acidity, *J. Chem. Soc. Chem. Commun.*, 1993, 676–678.

39   L. Lin, X. Zhang, N. He, J. Liu, Q. Xin, H. Guo, Operando dual beam FTIR study of hydroxyl groups and Zn species over defective HZSM-5 zeolite supported zinc catalysts, *Catalysts*, 2019, **9**, 100.

40   I. Halasz, B. Moden, A. Petushkov, J.J. Liang, M. Agarwal, Delicate distinction between OH groups on proton-exchanged H-chabazite and H-SAPO-34 molecular sieves, *J. Phys. Chem. C*, 2015, **119**, 24046–24055.

41   A.J. Liang, B.C. Gates, Time-resolved structural characterization of formation and break-up of rhodium clusters supported in highly dealuminated y zeolite, *J. Phys. Chem. C*, 2008, **112**, 18039–18049.

42   K. Torigoe, H. Remita, G. Picq, J. Belloni, D. Bazin, Structural characterization of supported platinum carbonyl clusters by X-ray absorption spectroscopy, *J. Phys. Chem. B*, 2000, **104**, 7050–7056.

43   M. Moliner, J.E. Gabay, C.E. Kliewer, R.T. Carr, J. Guzman, G.L. Casty, P. Serna, A. Corma, Reversible Transformation of Pt Nanoparticles into Single Atoms inside High-Silica Chabazite Zeolite, *J. Am. Chem. Soc.*, 2016, **138**, 15743–15750.

44   Y. Liu, Z. Li, Q. Yu, Y. Chen, Z. Chai, G. Zhao, S. Liu, W.C. Cheong, Y. Pan, Q. Zhang, L. Gu, L. Zheng, Y. Wang, Y. Lu, D. Wang, C. Chen, Q. Peng, Y. Liu, L. Liu, J. Chen, Y. Li, A General Strategy for Fabricating Isolated Single Metal Atomic Site Catalysts in Y Zeolite, *J. Am. Chem. Soc.*, 2019 **141**, 9305–9311.

45   Y. Akdogan, C. Vogt, M. Bauer, H. Bertagnolli, L. Giurgiu, E. Roduner, Platinum species in the pores of NaX, NaY and NaA zeolites studied using EPR, XAS and FTIR spectroscopies, *Phys. Chem. Chem. Phys.*, 2008 **10**, 2952–2963.

46   We infer that the CO present initially formed from the acac ligands in the Pt(acac)$_2$ precursor. Similar to reports of work with supported species formed from Rh(C$_2$H$_4$)$_2$(acac), we suggest that the SAPO OH groups might have reacted with the surface acac species, leading to the formation of acetates on the support and acetone in the gas phase. The small amount of acetone supposedly generated in-situ could then undergo decomposition on the platinum similar to that of reported to occur on rhodium to form a small amount of CO bonded to the platinum. Any gas-phase products such as acetone were evidently formed in amounts too low for detection with our on-line mass spectrometer.

47   V.A. Bhirud, J.O. Ehresmann, P.W. Kletnieks, J.F. Haw, B.C. Gates, Rhodium complex with ethylene ligands supported on highly dehydroxylated MgO: Synthesis, characterization, and reactivity, *Langmuir*, 2006, **22**, 490–496.

48   J.A. Anderson, C.H. Rochester, Infrared study of the adsorption of acetone, acrolein, ethanoic acid and propene-NO mixtures on Rh/Al$_2$O$_3$ catalysts, *J. Chem. Soc. Faraday Trans. 1*, 1989, **85**, 1117–1128.

49   K. Ding, A. Gulec, A.M. Johnson, N.M. Schweitzer, G.D. Stucky, L.D. Marks, P.C. Stair, Identification of active sites in CO oxidation and water-gas shift over supported Pt catalysts,

Science, 2015, **350**, 189–192.

50   K. Chakarova, M. Mihaylov, K. Hadjiivanov, FTIR spectroscopic study of CO adsorption on Pt-H-ZSM-5, *Micropor. Mesopor.Mater.*, 2005, **81**, 305–312.

51   H.A. Aleksandrov, K.M. Neyman, K.I. Hadjiivanov, G.N. Vayssilov, Can the state of platinum species be unambiguously determined by the stretching frequency of an adsorbed CO probe molecule?, *Phys. Chem. Chem. Phys.*, 2016, **18**, 22108–22121.

52   K.I. Hadjiivanov, G.N. Vayssilov, Characterization of oxide surfaces and zeolites by carbon monoxide as an IR probe molecule, *Adv. Catal.*, 2002, **47**, 307–511.

53   W.C. Conner, J.L. Falconer, Spillover in Heterogeneous Catalysis, *Chem. Rev.*, 1995, **95**, 759–788.

54   M.M. Bettahar, The hydrogen spillover effect. A misunderstanding story, *Catal. Rev. Sci. Eng.*, 2020, 1–39.

55   P. Serna, B.C. Gates, A bifunctional mechanism for ethene dimerization: Catalysis by rhodium complexes on zeolite HY in the absence of halides, *Angew. Chem. Ed.*, 2011, **50**, 5528–5531.

56   C. Martinez-Macias, P. Serna, B.C. Gates, Isostructural Zeolite-Supported Rhodium and Iridium Complexes: Tuning Catalytic Activity and Selectivity by Ligand Modification, *ACS Catal.*, 2015, **5**, 5647–5656.

57   R.M. Rioux, H. Song, J.D. Hoefelmeyer, P. Yang, G.A. Somorjai, High-surface-area catalyst design: Synthesis, characterization, and reaction studies of platinum nanoparticles in mesoporous SBA-15 silica, *J. Phys. Chem. B*, 2005, **109**, 2192–2202.

58   P. Gallezot, The State and Catalytic Properties of Platinum and Palladium in Faujasite-Type Zeolites, *Catal. Rev.*, 1979, **20**, 121–154.

59   A. Uzun, B.C. Gates, Dynamic structural changes in a molecular zeolite-supported iridium catalyst for ethene hydrogenation, *J. Am. Chem. Soc.*, 2009, **131**, 15887–15894.

60   P. Serna, B.C. Gates, Zeolite- and MgO-supported rhodium complexes and rhodium clusters: Tuning catalytic properties to control carbon-carbon vs. carbon-hydrogen bond formation

reactions of ethene in the presence of H$_2$, *J. Catal.*, 2013, **308**, 201–212.

61   E. Bus, D.E. Ramaker, J.A. van Bokhoven, Structure of ethene adsorption sites on supported metal

catalysts from in situ XANES analysis, *J. Am. Chem. Soc.*, 2007, **129**, 8094–8102.

62   A. Uzun, B.C. Gates, Real-time characterization of formation and breakup of iridium clusters in

highly dealuminated zeolite Y, *Angew. Chem. Int. Ed.*, 2008, **47**, 9245–9248.

63   J. De Graaf, A.J. Van Dillen, K.P. De Jong, D.C. Koningsberger, Preparation of highly dispersed

Pt particles in zeolite Y with a narrow particle size distribution: Characterization by hydrogen

chemisorption, TEM, EXAFS spectroscopy, and particle modeling, *J. Catal.*, 2001, **203**, 307–321.

64   J. Resasco, L. Derita, S. Dai, J.P. Chada, M. Xu, X. Yan, J. Finzel, S. Hanukovich, A.S. Hoffman,

G.W. Graham, S.R. Bare, X. Pan, P. Christopher, Uniformity Is Key in Defining Structure-

Function Relationships for Atomically Dispersed Metal Catalysts: The Case of Pt/CeO$_2$, *J. Am.*

Chem. Soc., 2020, **142**, 169–184.

65   V.L. Zholobenko, G.D. Lei, B.T. Carvill, B.A. Lerner, W.M.H. Sachtler, Identification of isolated

Pt atoms in H-mordenite, *J. Chem. Soc. Faraday Trans.*, 1994, **90**, 233–238.

66   P.S.F. Mendes, A.F.C. Gregório, A. Daudin, C. Bouchy, J.M. Silva, M.F. Ribeiro, Elucidation of

the zeolite role on the hydrogenating activity of Pt-catalysts, *Catal. Commun.*, 2017, **89**, 152–155.

67   C. Dessal, T. Len, F. Morfin, J.L. Rousset, M. Aouine, P. Afanasiev, L. Piccolo, Dynamics of

Single Pt Atoms on Alumina during CO Oxidation Monitored by Operando X-ray and Infrared

Spectroscopies, *ACS Catal.*, 2019, **9**, 5752–5759.

68   D. Yang, P. Xu, N.D. Browning, B.C. Gates, Tracking Rh Atoms in Zeolite HY: First Steps of

Metal Cluster Formation and Influence of Metal Nuclearity on Catalysis of Ethylene

Hydrogenation and Ethylene Dimerization, *J. Phys. Chem. Lett.*, 2016, **7**, 2537–2543.

69   J. Lu, P. Serna, C. Aydin, N.D. Browning, B.C. Gates, Supported molecular iridium catalysts:

Resolving effects of metal nuclearity and supports as ligands, *J. Am. Chem. Soc.*, 2011, **133**,

16186–16195.

70   J. Lu, C. Aydin, N.D. Browning, B.C. Gates, Hydrogen activation and metal hydride formation

trigger cluster formation from supported iridium complexes, *J. Am. Chem. Soc.*, 2012, **134**, 5022–5025.

71   J. Guzman, B.C. Gates, Structure and Reactivity of a Mononuclear Gold-Complex Catalyst Supported on Magnesium Oxide, *Angew. Chem. Int. Ed.*, 2003, **42**, 2001–2004.

72   X. Zhang, H. Shi, B.Q. Xu, Catalysis by gold: Isolated surface Au^{3+} ions are active sites for selective hydrogenation of 1,3-butadiene over Au/ZrO_2 catalysts, *Angew. Chem. Int. Ed.*, 2005, **44**, 7132–7135.

73   P. Serna, A. Rodríguez-Fernández, S. Yacob, C. Kliewer, M. Moliner, A. Corma, Single-Site vs. Cluster Catalysis in High Temperature Oxidations, *Angew. Chem. Int. Ed.*, 2021, **133**, 16090–16098.
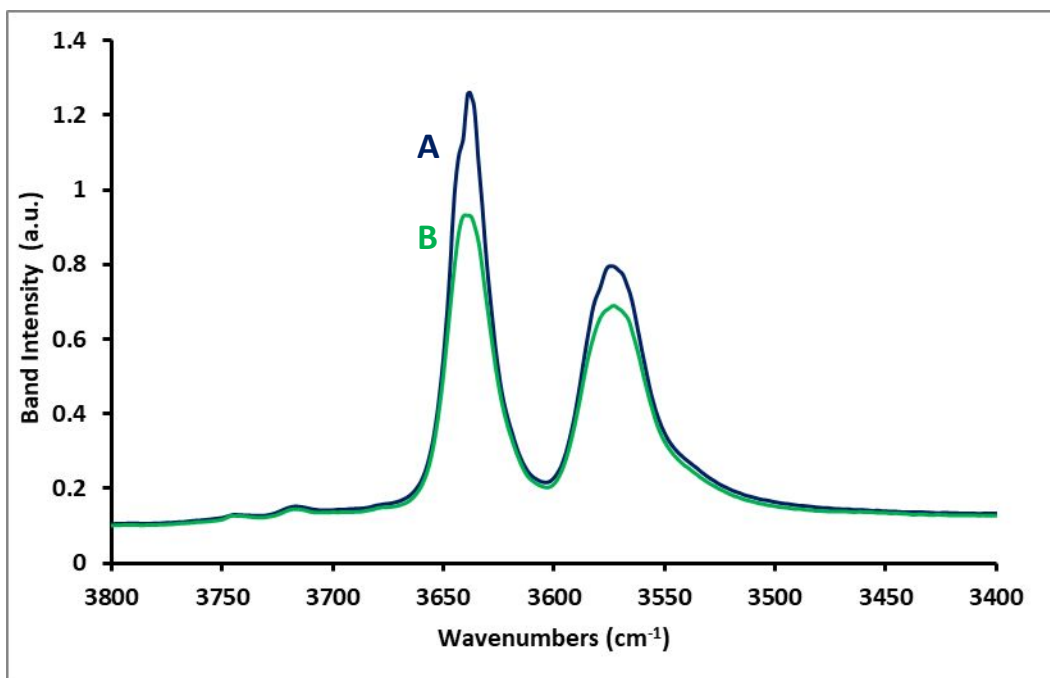
Fig. 1. IR spectra in the ν_{OH} region characterizing (**A**) calcined SAPO-37 and (**B**) sample formed by reaction of Pt(acac)$_2$ with calcined SAPO-37. The spectra were normalized with respect to the 600 cm^{-1} band characteristic of the SAPO framework.
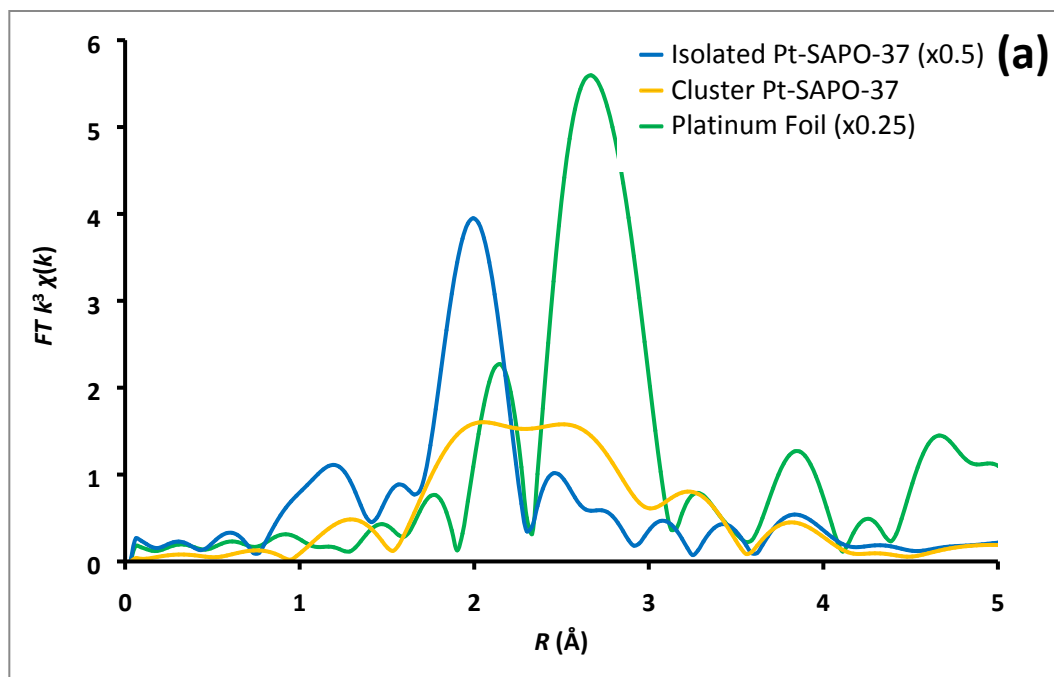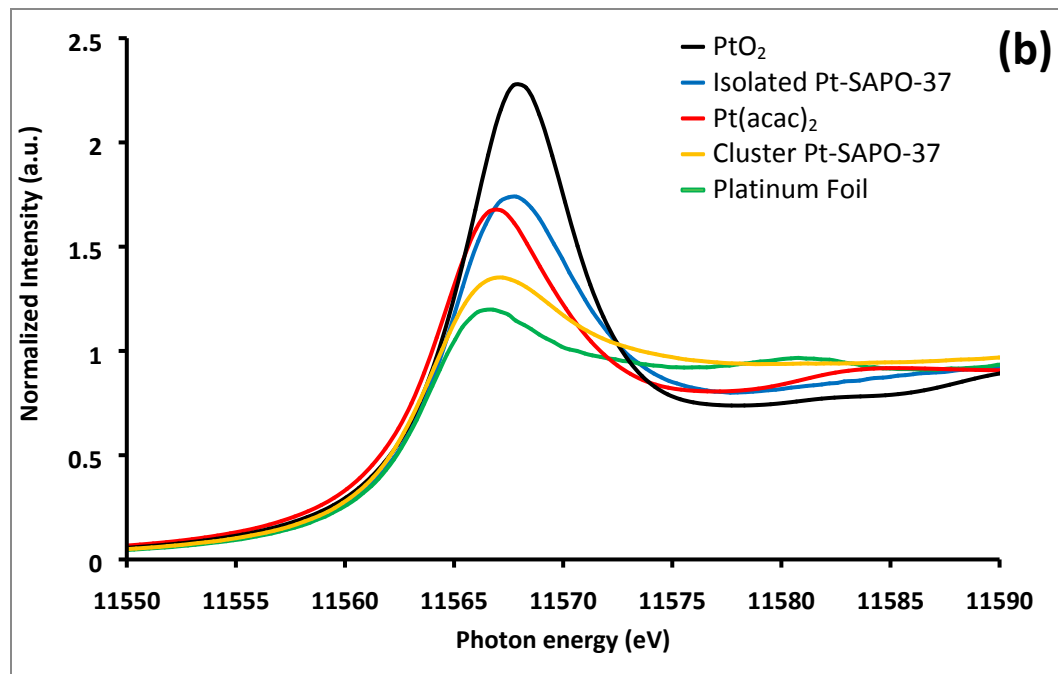
Fig. 2. (**a**) k^3-Weighted magnitude of the Fourier transforms of EXAFS data recorded at Pt L_{III}-edge characterizing SAPO-37-supported isolated platinum (blue), platinum clusters made from the isolated platinum species by exposure to H_2 (orange), and platinum foil (green). (**b**) XANES data characterizing platinum oxide (PtO_2, black), SAPO-37-supported isolated platinum (blue), $Pt(acac)_2$ (red), platinum clusters supported on SAPO-37 (orange), and platinum foil (green).
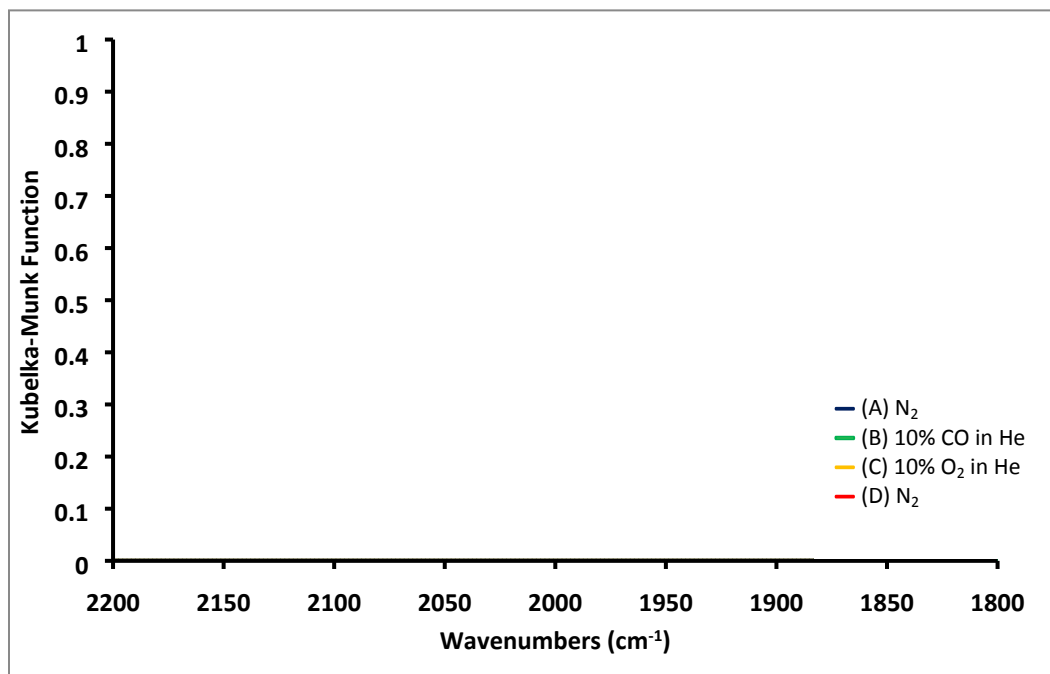
Fig. 3. DRIFTS data in the ν_{CO} region: (**A**) recorded with the initially prepared sample (after the oxidation synthesis) in N_2 flowing at 50 mL(NTP)/min; (**B**) recorded after sample had been in contact with flowing 10% CO in helium for 15 min, followed by a purge of the DRIFTS cell with helium for 30 min; (**C**) recorded after exposure to 10% O_2 at 473 K of sample in helium flowing at 50 mL(NTP)/min; and (**D**) recorded following these treatments with sample at room temperature in flowing N_2.
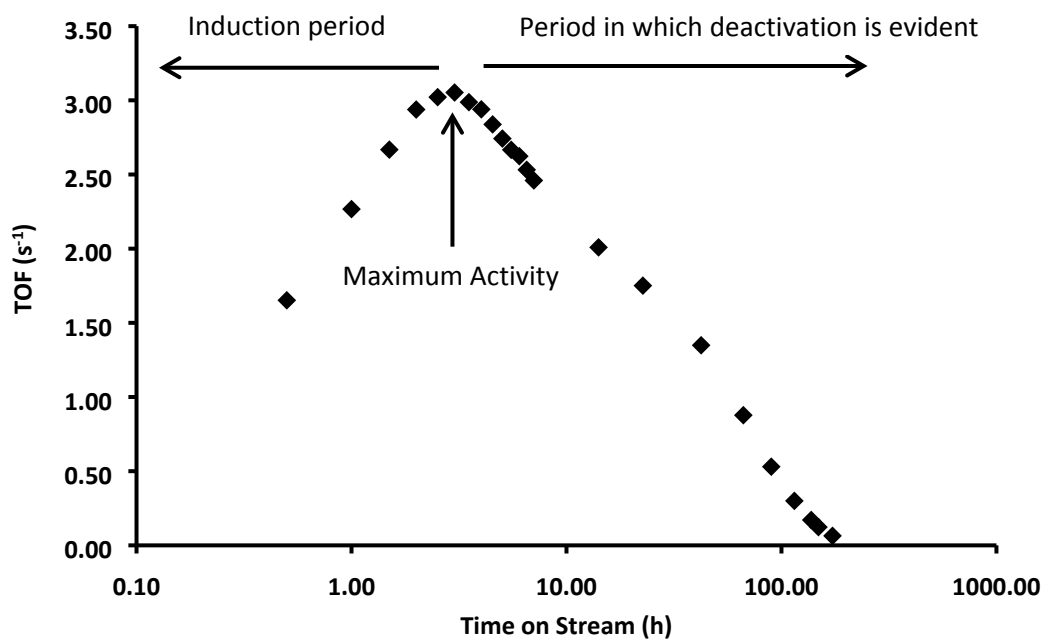
Fig. 4. Performance of platinum supported on SAPO-37 for ethylene conversion catalysis in a once-through plug-flow reactor in the presence of H_2 at 303 K and 1 bar (molar $H_2:C_2H_4$ ratio = 10:1). The catalyst contained 1.1 ± 0.1 wt% platinum, and the TOF values were determined on the basis of the assumption that each platinum atom was exposed at each stage of the flow-reactor operation; see text for interpretation of how deactivation occurred and Table 2 for estimated error in TOF values.
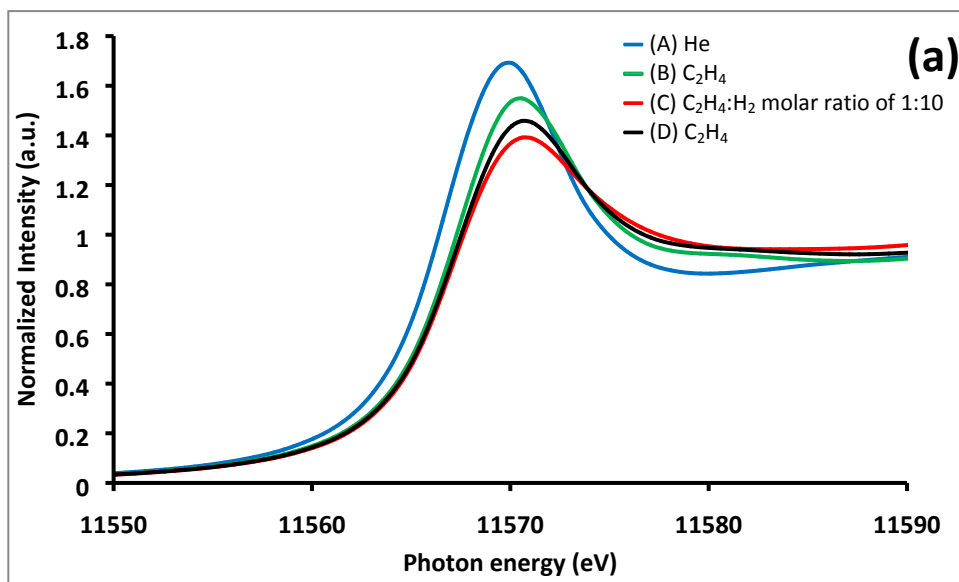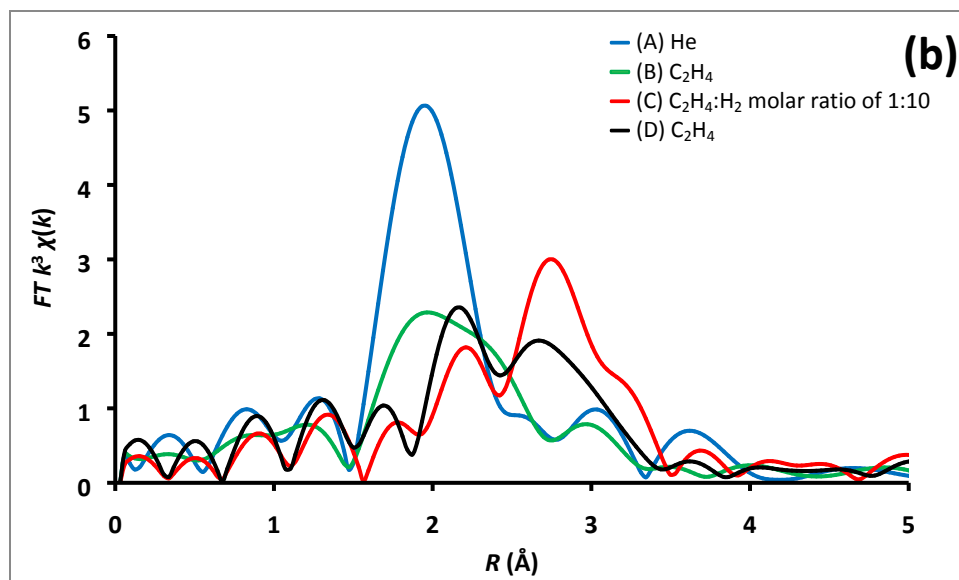
Fig. 5. (a) XANES data characterizing SAPO-37-supported platinum complexes under the following conditions: (A) initial isolated platinum complexes (after oxidation synthesis) in flowing helium (30.0 mL(NTP) min⁻¹) (blue); (B) the sample subsequently exposed to flowing ethylene flowing at a rate of 2.4 mL(NTP) min⁻¹ (green); (C) the sample subsequently under catalytic reaction condtions (C_2H_4:H_2 molar ratio = 1:10) (red); (D) the sample after a subsequent 2-h exposure to ethylene flowing at a rate of 2.4 mL(NTP) min⁻¹ (black). (b) k^3-Weighted magnitude of the Fourier transforms of the EXAFS data recorded at the Pt L_{III}-edge characterizing SAPO-37-supported platinum complexes under conditions stated in (a).
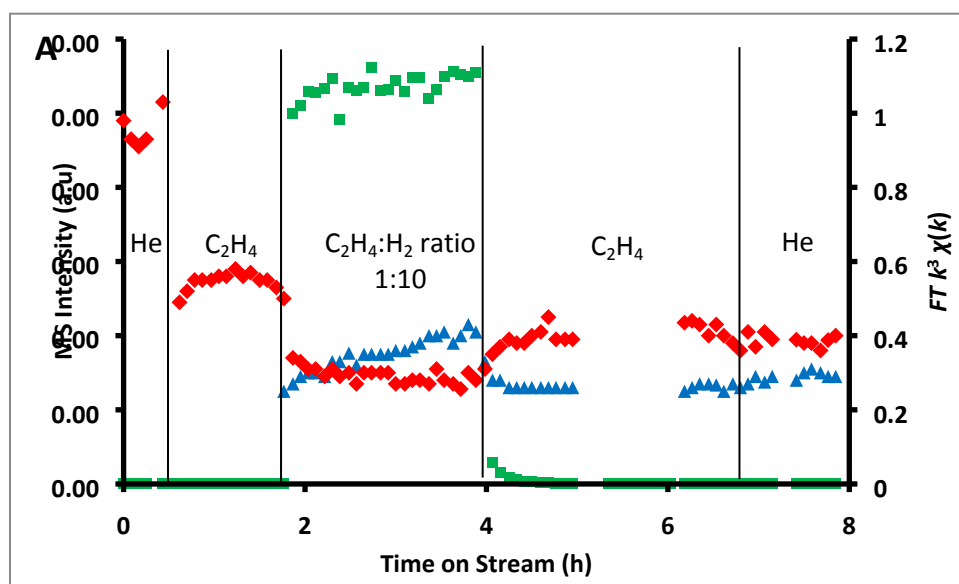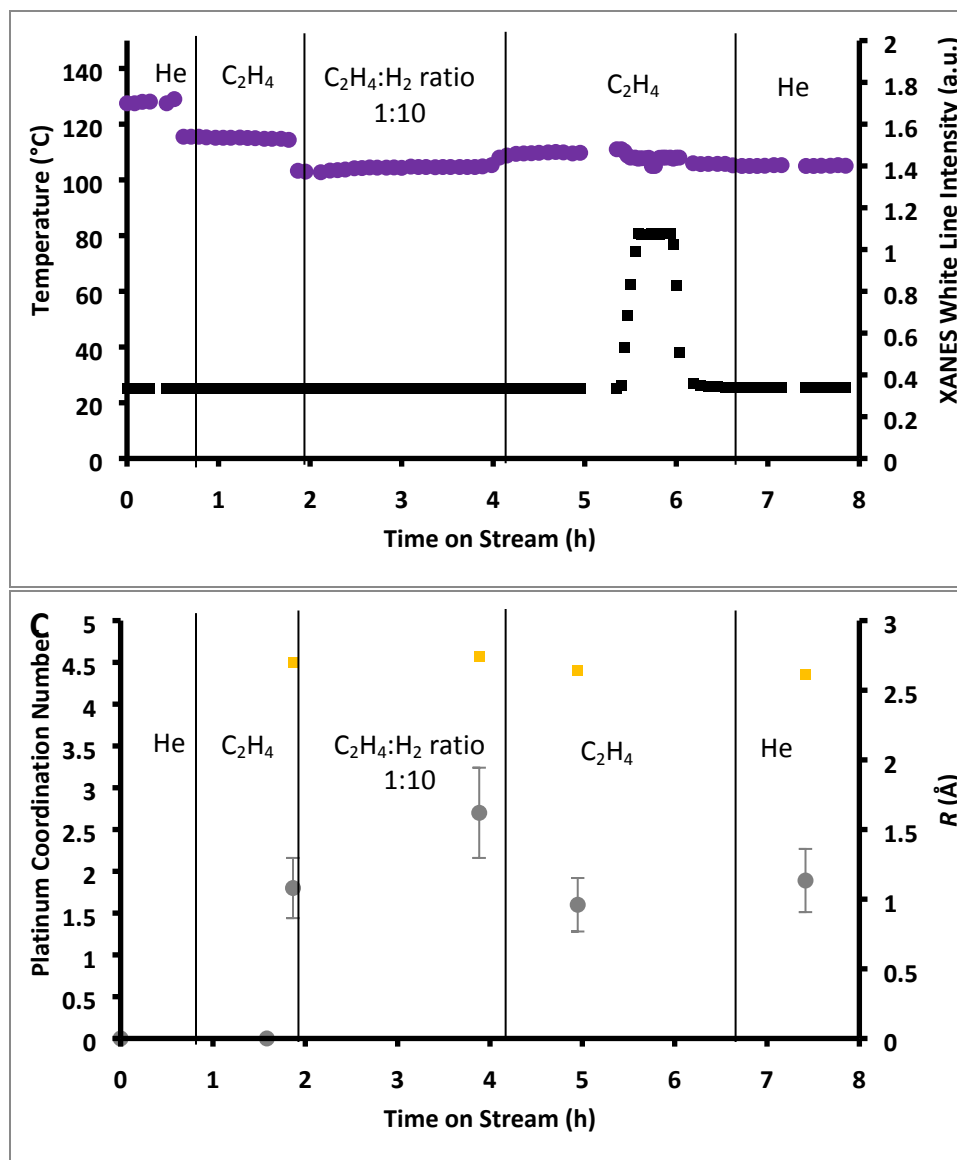

B

Fig. 6. (a) Changes in k^3-weighted magnitude of the Fourier transforms of the EXAFS data and ethane signal observed during operation of the catalyst (1.1 ± 0.1 wt% platinum supported on SAPO-37) under ethylene hydrogenation conditions (molar H_2:C_2H_4 ratio = 10:1) in the EXAFS cell at 303 K and 1 bar. Symbols: red ◆, Pt−light-scatterer contribution at 2 Å; blue ▲, Pt−Pt contribution 2.5−2.8 Å; green ■, mass spectra of ethane ($m/z = 30$) in the effluent gas. (b) Changes in the white line intensity and temperature in various reactive gases. Symbols: purple •, white line intensity; black ■, temperature. **(c)** Changes in the Pt−Pt distance and coordination number with sample in various reactive gases. Symbols: gray •, platinum coordination number; orange ■, Pt−Pt distance. Details are presented in the text.